


Coupling and protection effects of Jackiw-Rebbi states and trivial states in interfaced binary waveguide arrays

Truong X. Tran*

Department of Physics, Le Quy Don Technical University, 236 Hoang Quoc Viet Street, 10000 Hanoi, Vietnam

 (Received 10 February 2020; accepted 1 June 2020; published 19 June 2020)

We systematically study different scenarios of interaction between two localized structures which were both found recently in interfaced binary waveguide arrays with alternating signs of the Dirac mass in the linear and nonlinear regimes of Kerr type. The first localized structure is the optical analog of the famous Jackiw-Rebbi state emerging from the Dirac equation in quantum field theory, and the second one is the trivial state. We show that two localized states of different types practically do not interact at all; thus, they can be protected from each other in a reliable way. Meanwhile, two localized states of the same type can couple efficiently with each other and show the nonlinear switching effect like in well-known symmetric fiber couplers.

DOI: [10.1103/PhysRevA.101.063826](https://doi.org/10.1103/PhysRevA.101.063826)

I. INTRODUCTION

Many interesting optical effects, e.g., discrete diffraction [1,2], discrete solitons [1,3,4], diffractive resonant radiation [5], soliton self-wave-number shift [6], and the supercontinuum generation in both frequency and wave-number domains [7], exist in waveguide arrays (WAs). This platform has also been used to mimic fundamental phenomena in nonrelativistic quantum mechanics, for example, Bloch oscillations [8] and Zener tunneling [9]. However, in order to investigate relativistic quantum mechanics phenomena arising from the Dirac equation one needs to use binary waveguide arrays (BWAs). Indeed, BWAs have been widely exploited to mimic *Zitterbewegung* [10,11], Klein tunneling [12,13], Dirac solitons in both one-dimensional (1D) [14–16] and two-dimensional (2D) cases [17]. The Dirac light bullet conserving its spatiotemporal profile can also exist in BWAs [18]. The routing of a Dirac soliton with the help of another very weak beam in BWAs possessing variable propagation mismatch was reported in Ref. [19]. The latter model can help to simulate the Dirac equation in curved space-time. In the classical context, the discrete gap solitons in BWAs were observed earlier [20–23]. The linear surface states and nonlinear surface modes existing at the edge of BWAs have also been found in Ref. [24].

Recently, two localized states—one is the optical analog of the well-known *Jackiw-Rebbi* (JR) state emerging from the Dirac equation in the quantum field theory [25], and the other is the trivial state—were found at the interface of two BWAs with opposite propagation mismatches in the linear regime in Ref. [26]. In the nonlinear regime, the exact profiles and the detunings of these two localized states can be numerically found by using the shooting method [27], as reported quite recently in Ref. [28] for Kerr nonlinearity and in Ref. [29] for cubic-quintic nonlinearity. The interaction between Dirac solitons and JR states in BWAs were studied in Ref. [30]. The

JR state is fundamental in predicting the charge fractionalization effect, which has a central role in the fractional quantum Hall effect [31]. The topological nature of the JR-state zero-energy solution is fundamental to topological insulators [32]. Topological photonics can potentially play a crucial role in the design of extremely stable optical circuits [33]. Quite recently, the JR states in BWAs were numerically demonstrated to be also very stable with respect to strong disturbances of various kinds, e.g., the switching on or off of the nonlinearity, the oblique incidence, and the linear transverse potential [34]. Photonic topological defect modes at the edge of BWAs were demonstrated in Ref. [35]. Topological defect states existing at the interface between two periodic dimer chains were reported in Ref. [36]. Up to now, some models have been used to investigate JR states, for example, in a periodic photonic lattice with the use of an atomic Fermi-Dirac gas [37] or in a fermionic superfluid with so-called heavy solitons [38]. An optical realization of JR states in a polaritonic scheme possessing the slow-light effect was analyzed in Ref. [39]. Jackiw-Rebbi states occurring on a dislocation in a 2D photonic crystal were studied in Ref. [40]. The photonic JR states in the all-dielectric platform with bianisotropy were studied in Ref. [41], and the plasmonic JR modes in graphene waveguide arrays were studied in Ref. [42].

In this work we study the interaction between two localized states—one is the JR state, and the other is the trivial state—in BWAs made of material with Kerr nonlinearity found in Ref. [26]. We show that two localized states of the same type can couple efficiently and exhibit the nonlinear switching effect like in fiber couplers, whereas two localized states of different types practically do not interact with each other at all.

II. THEORETICAL BACKGROUND AND SOLUTIONS OF JR AND TRIVIAL STATES IN THE LINEAR REGIME

In this section, we briefly reintroduce the principal equations in interfaced BWAs and the *linear* exact solutions of localized states already reported in Ref. [26] in 2017.

*tranxtr@gmail.com

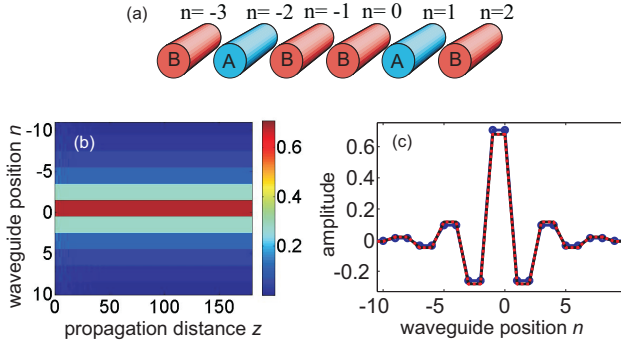


FIG. 1. (a) A system of two BWAs adjacent to each other with opposite propagation mismatches. (b) Evolution of a linear JR state in BWAs where continuous equation (3) is exploited to calculate the input condition. (c) The solid blue curve with round markers shows the profile of the input beam, whereas the solid black curve plots the output profile. The latter curve is hidden by the dotted red curve showing the discrete solution (4). Parameters are $-\sigma_1 = \sigma_2 = 1$, $\kappa = 1$, $\gamma = 0$. Reproduced from Fig. 1 in Ref. [26].

Light-beam evolution in BWAs with Kerr nonlinearity can be studied by dimensionless coupled-mode equations as follows [20]:

$$i \frac{da_n(z)}{dz} + \kappa[a_{n+1} + a_{n-1}] - (-1)^n \sigma a_n + \gamma |a_n|^2 a_n = 0, \quad (1)$$

where a_n is the electric amplitude in the waveguide with discrete position n , z is the longitudinal spatial coordinate, κ and 2σ are the coupling coefficient and the propagation mismatch of two neighboring waveguides in BWAs, respectively, and γ is the nonlinear coefficient of waveguides. Now let us briefly reintroduce the localized solutions obtained at the interface of two BWAs with opposite propagation mismatches which were found earlier in Ref. [26]. To be specific, for now we set this interface at two waveguides with $n = (-1, 0)$, as shown Fig. 1(a). At waveguides with $n < 0$ one has $\sigma = \sigma_1$, whereas at waveguides with $n \geq 0$ one has $\sigma = \sigma_2$. After setting $\Psi_1(n) = (-1)^n a_{2n}$ and $\Psi_2(n) = i(-1)^n a_{2n-1}$, one can now introduce the continuous transverse coordinate ξ instead of n and the two-component spinor $\Psi(\xi, z) = (\Psi_1, \Psi_2)^T$, which satisfies the 1D nonlinear Dirac equation [14]:

$$i \partial_z \Psi = -i \kappa \hat{\sigma}_x \partial_\xi \Psi + \sigma \hat{\sigma}_z \Psi - \gamma G, \quad (2)$$

where the last term $G \equiv (|\Psi_1|^2 \Psi_1, |\Psi_2|^2 \Psi_2)^T$ accounts for the Kerr nonlinearity; $\hat{\sigma}_x$ and $\hat{\sigma}_z$ are the standard Pauli matrices. Parameter σ is the so-called mass of the Dirac field in quantum field theory. We want to emphasize that the Dirac equation (2) can be derived only from the discrete equations (1) under a crucial requirement for discrete solutions a_n such that the derivative $\partial_\xi \Psi$ in Eq. (2) mathematically makes sense (see also Sec. V in Ref. [17] for more details).

If $\sigma_1 < 0$ and $\sigma_2 > 0$, one obtains the continuous linear JR solution of Eq. (2) as follows: [26]:

$$\Psi(\xi) = \sqrt{\frac{|\sigma_1 \sigma_2|}{\kappa(|\sigma_1| + |\sigma_2|)}} \begin{pmatrix} 1 \\ i \end{pmatrix} e^{-|\sigma(\xi)|\xi/\kappa}. \quad (3)$$

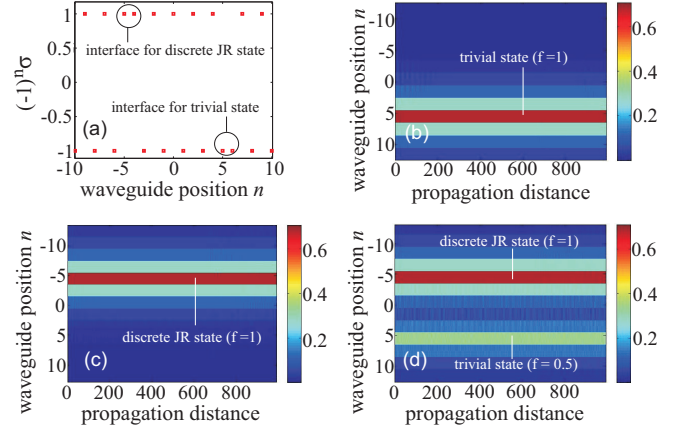


FIG. 2. Interaction of two localized states of different types interfaced BWAs in the linear regime. (a) The array of $(-1)^n \sigma$ which is used to investigate the interaction of two localized states of different types in interfaced BWAs. (b) Only the trivial state is launched into the system at the input. (c) Only the discrete JR state is launched into the system at the input. (d) Two localized states of different types with different initial peak amplitudes are launched into the system. Parameters are $-\sigma_1 = \sigma_2 = -\sigma_3 = 1$, $\kappa = 1$, $\gamma = 0$.

If $|\sigma_1| = |\sigma_2| = \sigma_0$, as reported in Ref. [26], we obtain exact linear localized solutions for the discrete equations (1) in two cases as follows:

First, if $-\sigma_1 = \sigma_2 = \sigma_0 > 0$ [i.e., $\sigma_1 < 0$ and $\sigma_2 > 0$ as required to get the continuous JR solution (3)], we obtain the discrete linear JR-state solution [26]:

$$a_n = b_n e^{i \delta_1 z}, \quad (4)$$

where the detuning $\delta_1 \equiv \kappa - \sqrt{\sigma_0^2 + \kappa^2}$ and b_n has a real value and is independent of z , $b_{2n-1} = b_{2n}$. For $n \geq 0$ we have the following relationship: $b_{2n}/b_{2n+1} = \alpha \equiv -[\sigma_0/\kappa + \sqrt{1 + \sigma_0^2/\kappa^2}]$. Meanwhile, for $n < 0$ we have $b_{2n+1}/b_{2n} = \alpha$. It is worth emphasizing that to support discrete JR states, two neighboring waveguides at the interface need to have positive values for $(-1)^n \sigma$ [see also Fig. 2(a) for more details]. Note also that the linear detuning δ_1 is always negative because $\kappa > 0$. It is also worth mentioning that from this discrete solution b_n , the component $\Psi_1(n)$ can be straightforwardly constructed and always possesses the same sign for all values of n (after removing the common factor $e^{i \delta_1 z}$). The component $\Psi_2(n)$ also possesses this feature. As a result, the derivative $\partial_\xi \Psi$ in Eq. (2) mathematically exists. Therefore, in this case one can say that the discrete solution in the form of Eqs. (4) is the approximate JR-state solution to the continuous Dirac equation (2).

Second, if $\sigma_1 = -\sigma_2 = \sigma_0 > 0$, we get the trivial localized state solution as follows [26]:

$$a_n = b_n e^{i \delta_2 z}, \quad (5)$$

where the detuning $\delta_2 \equiv \kappa + \sqrt{\sigma_0^2 + \kappa^2}$ and b_n also has a real value and is independent of z , $b_{2n-1} = b_{2n}$. If $n \geq 0$ we have $b_{2n}/b_{2n+1} = -\alpha$. Meanwhile, for $n < 0$ we have $b_{2n+1}/b_{2n} = -\alpha$. It is worth recalling that to support trivial states, two neighboring waveguides at the interface need to have negative

values for $(-1)^n \sigma$ [see also Fig. 2(a) for more details]. Note also that the linear detuning δ_2 is always *positive* because $\kappa > 0$. It is important to stress that this discrete solution b_n leads to the construction of the component $\Psi_1(n)$ with *opposite* signs for adjacent values of n (after removing the common factor $e^{i\delta_1 z}$), i.e., $\Psi_1(n) \cdot \Psi_1(n+1) \leq 0$ for every value of n . The component $\Psi_2(n)$ also possesses this features. As a result, the derivative $\partial_\xi \Psi$ in Eq. (2) does not have a mathematical sense. Therefore, one *cannot* say that the discrete solution (5) is the approximate JR solution to the continuous Dirac equation (2). Instead, the discrete solution in the form of Eqs. (5) is just a trivial localized solution to Eqs. (1).

The scheme of two adjacent BWAs with opposite propagation mismatches is illustrated in Fig. 1(a). Figure 1(b) shows the evolution of a linear JR state where the continuous JR solution (3) is used to calculate the initial condition for integrating Eqs. (1). The solid blue curve with round markers in Fig. 1(c) is the input JR-state profile, whereas the solid black curve shows the output JR-state profile. The dotted red curve showing the exact discrete JR solution (4) to Eq. (1) is also plotted in Fig. 1(c) for comparison. As seen in Fig. 1(c), the latter curve coincides perfectly with the output solid black curve. As a result, one cannot clearly see the output curve. This feature shows that the discrete solution in the form of Eqs. (4) is an authentic JR state, indeed.

Because the solutions in the form of Eqs. (3)–(5) are obtained in the linear case, obviously, we will get other linear solutions if we multiply them by an arbitrary number. In other words, the peak amplitudes of linear solutions can be chosen arbitrarily. In the rest of this work, we numerically solve Eqs. (1) to investigate the interaction between two localized states in interfaced BWAs. As initial conditions for this task we mostly use beams in the form of Eqs. (3), (4), and (5) multiplied by a certain factor f which will be specified later in each case. The only exception for initial conditions takes place in Sec. IV, where we use an exact nonlinear JR-state solution at the input to study the interaction of two nonlinear JR states.

III. INTERACTION OF THE JR STATE WITH THE TRIVIAL STATE IN THE LINEAR REGIME

Now it is time for us to investigate the interaction of two localized states in interfaced BWAs. First, we analyze the interaction of two localized states of different types, as shown in Fig. 2 in the *linear* regime ($\gamma = 0$). Figure 2(a) plots the array of $(-1)^n \sigma$, where the interface at two waveguides with $n = (-5, -4)$ can generate a JR discrete state, whereas the interface at two waveguides with $n = (5, 6)$ can generate a trivial state. The system consists of three BWAs: the first one covers all waveguides with $n \leq -5$ and has the propagation mismatch parameter σ_1 , the second one covers all waveguides with $-4 \leq n \leq 5$ and has the propagation mismatch parameter σ_2 , and the third one covers all waveguides with $n \geq 6$ and has the propagation mismatch parameter σ_3 . Figure 2(b) shows the propagation of a trivial state at the interface with $n = (5, 6)$, and one can clearly see that this trivial state does not generate any signal at the other interface with $n = (-5, -4)$, even though these two interfaces are located quite close to each other. Similarly, Fig. 2(c) shows

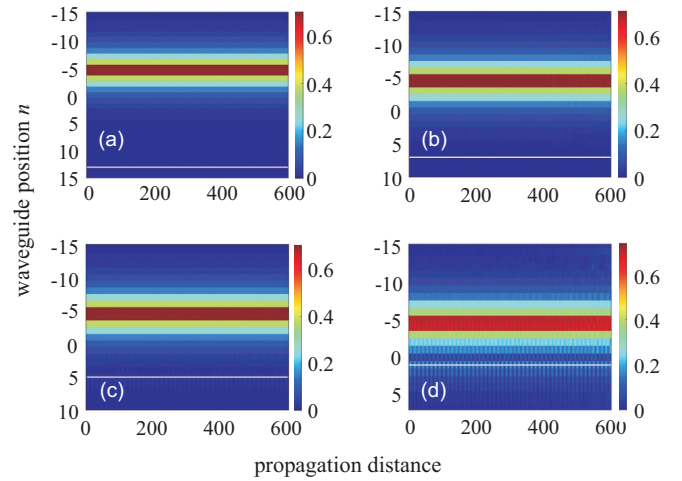


FIG. 3. Protection of a discrete JR state in the nonlinear regime from being coupled to trivial states. The exact nonlinear discrete JR state is launched into the system at the interface with $n = (-5, -4)$. The white lines indicate the position of the interface for the trivial state with (a) $n = (13, 14)$, (b) $(7, 8)$, (c) $(5, 6)$, and (d) $(1, 2)$. All parameters are the same as in Fig. 2 except for $\gamma = 1$ now.

that if one launches a discrete JR state into the interface with $n = (-5, -4)$, no signal will be generated at the other interface with $n = (5, 6)$. Thus, the localized states of one type cannot generate the localized states of the other type, even if the interfaces supporting these localized states are quite close to each other. Now we launch at the same time two localized states of different types, as shown in Fig. 2(d); we can see that these two localized states of different types practically do not interact at all, although they are quite close to each other. Each localized state in Fig. 2(d) propagates practically independently of the other and maintains its shape quite well during propagation.

Physically, the reason two linear localized states of different types cannot couple or interact with each other can be easily explained. Indeed, as shown in Eqs. (4) and mentioned in Sec. II, the detuning δ_1 of the linear discrete JR states always has a *negative* value. However, as shown in Eqs. (5) and mentioned in Sec. II, the detuning δ_2 of the linear trivial state always has a *positive* value. So these two linear localized states of different types cannot be phase matched during propagation. As a result, they cannot couple to each other.

To estimate real physical quantities, let us use common parameters in WAs made of AlGaAs [43], where in physical units the nonlinear coefficient is $\Gamma = 6.5 \text{ m}^{-1} \text{ W}^{-1}$ and the coupling coefficient is $K = 1240 \text{ m}^{-1}$. So the power scale is $P_0 = K/\Gamma = 190.8 \text{ W}$; thus, the JR-state peak power in Fig. 2 is around 70 W, and the length scale in the longitudinal direction is $z_0 = 1/K = 0.8 \text{ mm}$.

IV. INTERACTION OF THE JR STATE WITH THE TRIVIAL STATE IN THE NONLINEAR REGIME

In Fig. 2 we show that, in the linear regime, localized states of different types do not interact with each other. It turns out that this feature also takes place in the *nonlinear* regime, i.e., when $\gamma \neq 0$, as shown in Fig. 3, where we launch an exact

nonlinear discrete JR state into the system at the interface with $n = (-5, -4)$ and check if this discrete JR state can generate trivial states at other interfaces indicated by the white lines in Fig. 3. The interface for the trivial states in Figs. 3(a)–3(d) is located at waveguides with $n = (13, 14)$, (7, 8), (5, 6), and (1, 2), respectively. Note that the array for $(-1)^n \sigma$ is the same as in Fig. 2(a), with the only exception being that the position of the interface supporting trivial states is varied. To get initial conditions, the shooting method is exploited to numerically obtain the exact nonlinear discrete JR state with the peak amplitude $a_{-5} = a_{-4} = 0.7$ at the input (see Ref. [28] for more details). This initial condition is calculated by assuming that there is just *one* interface at waveguides $n = (-5, -4)$ in the whole system. With this value for the discrete JR-state peak amplitude and with parameters used in Fig. 3, the eigenvalue for the detuning of this JR state is calculated to be $\delta = 0.1105\delta_1 = -0.0458$.

Like in the linear case illustrated in Fig. 2, it is also clearly shown in Fig. 3 that in the nonlinear regime the nonlinear discrete JR state at the interface with $n = (-5, -4)$ cannot generate the trivial states at nearby interfaces. Indeed, in Fig. 3(a) the two interfaces are far from each other, so as expected, the discrete JR state can perfectly conserve its profile during propagation without being disturbed by the presence of the second interface at $n = (13, 14)$ like what happens to nonlinear discrete JR states in the ideal condition analyzed in Ref. [28], where the array consists of only one interface. In Figs. 3(b) and 3(c) the two interfaces are located closer to one another, but the influence of the interface supporting trivial states on the dynamics of the discrete JR state is so negligible that one can see only some extremely weak fluctuation in its profile during propagation just by zooming in on Figs. 3(b) and 3(c). Even when the interface supporting trivial states is quite close to the site of the discrete JR state as in Fig. 3(d), we can see only that some weak signal at the interface with $n = (1, 2)$ is periodically generated during propagation. However, the amplitude of this signal is also small and just a bit larger than the amplitude of the signal at the opposite site of the discrete JR state, i.e., at $n = (-11, -10)$.

So one can say that in the nonlinear regime, the discrete JR state is also protected quite well from being coupled to the other nearby interfaces supporting trivial states. This is also based on the fact that the phase-matching condition for two nonlinear localized states of different types cannot be satisfied with all the data that we already showed previously in Fig. 3 in Ref. [28] and that are reproduced here for convenience in Fig. 4, where we show the relative detuning δ/δ_1 for nonlinear JR states [Fig. 4(a)] and the relative detuning δ/δ_2 for nonlinear trivial states [Fig. 4(b)] as a function of the peak amplitude b_0 for several sets of parameters. Indeed, the detuning for the nonlinear discrete JR state in Fig. 3 is $\delta = 0.1105\delta_1 = -0.0458$ (as indicated above), whereas all the eigenvalues of the detuning for nonlinear trivial states are positive, as shown in Fig. 4(b). Note that, as mentioned in Sec. II, δ_1 is always negative, whereas δ_2 is always positive. Of course, one can use other parameters to get a discrete JR state with a positive detuning, as shown in Fig. 4(a). However, even in that case we are still not able (with all the data we show in Fig. 4) to find a situation where the localized states of different types can be phase matched, i.e., when they have the

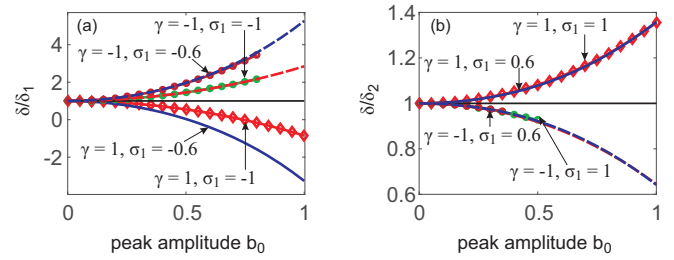


FIG. 4. (a) Relative detuning δ/δ_1 of nonlinear discrete JR states as a function of the peak amplitude b_0 . (b) Relative detuning δ/δ_2 of nonlinear trivial states as a function of b_0 . Reproduced from Fig. 3 in Ref. [28].

same value for the detuning δ . Probably, with the behaviors of all curves for detuning shown in Fig. 4, we guess that for self-focusing materials this phase-matching condition can be realized if the discrete JR-state peak amplitude is much larger than unity and the trivial-state peak amplitude is small, around zero, at the same time. Note also that, as shown in Refs. [28,29], both JR states and trivial states in interfaced BWAs are distinguished from all localized structures in other systems in the sense that both the transverse dimension and peak amplitude of localized states in interfaced BWAs can increase (or decrease) at the same time. So, in any case, the coupling of two localized states of different types in both the linear and nonlinear regimes is quite weak. This demonstrates that if a system of BWAs has two interfaces supporting localized states of different types, then each localized state propagating at one interface can be protected from escaping or coupling to the other interface, even if these interfaces are located quite close to each other, as shown in Fig. 3. Note that in Fig. 3 we demonstrate that a nonlinear discrete JR state cannot be coupled to a nearby interface supporting trivial states. In the same way, our simulations (not included here) also show that a nonlinear trivial state cannot be coupled to a nearby interface supporting JR states.

V. INTERACTION OF TWO LOCALIZED STATES OF THE SAME TYPE

The situation completely changes if two localized states are of the same type, as demonstrated in Fig. 5. To be specific, in Fig. 5 we investigate the interaction of two discrete JR states. Figure 5(a) plots the array of $(-1)^n \sigma$, where the two interfaces—one at waveguides with $n = (-5, -4)$ and the other at waveguides with $n = (4, 5)$ —can both generate discrete JR states. So in this case the center-to-center distance between these two interfaces is $D = 9$. The system consists of three BWAs: the first one covers all waveguides with $n \leq -5$ and has the propagation mismatch parameter σ_1 , the second one covers all waveguides with $-4 \leq n \leq 4$ and has the propagation mismatch parameter σ_2 , and the third one covers all waveguides with $n \geq 5$ and has the propagation mismatch parameter σ_3 . In Fig. 5(b) we launch a discrete JR state with $f = 0.1$ at the interface with two waveguides $n = (4, 5)$. Unlike the situation in Figs. 2(b) and 2(c), one now can clearly see the coupling between two discrete JR states in Fig. 5(b) with the coupling length $L \simeq 106$, where all the

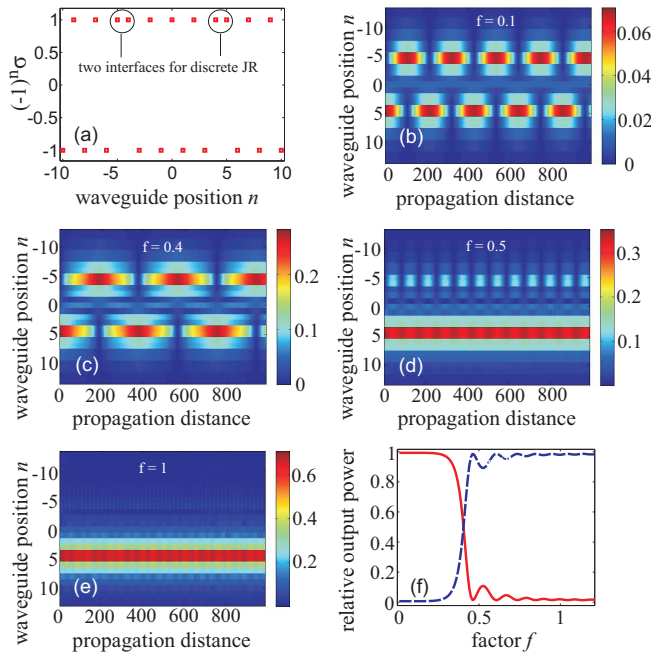


FIG. 5. Coupling of two discrete JR states. (a) The array of $(-1)^n \sigma$ as a function of the waveguide position n . (b)–(e) Coupling of two discrete JR states when $f = 0.1, 0.4, 0.5$, and 1.0 , respectively. (f) The switching character of two discrete JR states when the longitudinal length of BWAs is equal to the linear coupling length $L \simeq 106$. Parameters are $-\sigma_1 = \sigma_2 = -\sigma_3 = 1$, $\kappa = 1$, $\gamma = 1$.

energy of the discrete JR state at the interface with $n = (4, 5)$ is transferred to the discrete JR state at the interface with $n = (-5, -4)$. At the propagation distance $z = 2L$ all the energy is again completely transferred back to the initial discrete JR state at the interface with $n = (4, 5)$. This kind of energy transfer (or coupling) between the two discrete JR states takes place periodically. It is worth mentioning that although in Fig. 5 we use the nonlinear coefficient $\gamma = 1$, in Fig. 5(b) the factor $f = 0.1$ is very small; therefore, all qualitative and quantitative features in Fig. 5(b) are also reproduced exactly in the linear regime ($\gamma = 0$). This linear coupling between two discrete JR states is completely similar to the well-known coupling between signals in two cores of a symmetric fiber coupler [4]. The physics behind the coupling between two discrete JR states can be easily understood because, as clearly seen in their analytical solutions in the form of Eqs. (4), in the linear (or low-power) regime these states always have the same detuning δ_1 , provided that $|\sigma_1| = |\sigma_2| = |\sigma_3|$ and the coupling coefficient κ is constant for the whole system. In this case, the phase-matching condition during propagation between these discrete JR states in the linear regime is always fulfilled, which results in efficient coupling between them.

In Fig. 5(c) the factor f is increased up to the value $f = 0.4$. One can clearly see that all qualitative features in Fig. 5(b) also take place in Fig. 5(c), with the only exception being that the coupling length in Fig. 5(c) is $L \simeq 190$ instead of $L \simeq 106$ in Fig. 5(b). This increase in the nonlinear coupling length between two discrete JR states in the nonlinear regime is also similar to what happens in a symmetric fiber coupler

in the nonlinear regime when the input power P_0 is smaller than the so-called critical power P_c (see Ref. [4], p. 63, for more details). Note that if we set $\gamma = 0$ in getting results for Fig. 5(c), then the coupling length L must also be equal to $L \simeq 106$ as in the low-power linear regime illustrated in Fig. 5(b).

In Fig. 5(d) we increase further the factor f up to the value $f = 0.5$. Now the beam dynamics is again periodic during propagation, but only a small amount of the total energy is periodically transferred to the interface with $n = (-5, -4)$, whereas the main part of the total energy is trapped at the interface with $n = (4, 5)$. This situation is totally different from the scenarios in Figs. 5(b) and 5(c) where all energy is periodically transferred between the two interfaces. This behavior of nonlinear coupling between two discrete JR states is again completely similar to the nonlinear coupling scenario in symmetric fiber couplers when the input power P_0 is larger than the critical power P_c (see Ref. [4], p. 63).

In Fig. 5(e) we increase further the factor f up to the value $f = 1$. Now the input discrete JR state is trapped at the interface with $n = (4, 5)$ that it was launched into. This case is again similar to the trapping effect in symmetric fiber couplers when $P_0 \gg P_c$ [4]. Therefore, like in fiber couplers, a discrete JR state can be transferred from one interface to the other or trapped at one interface, depending on its input power, provided that these two interfaces are able to generate discrete JR states.

In Fig. 5(f) we plot the relative output power of the two discrete JR states (with respect to the total initial input power) at a propagation distance equal to the linear coupling length $L \simeq 106$ as a function of the factor f . The input discrete JR state is launched at the interface with $n = (4, 5)$. The solid red curve and the dashed blue one in Fig. 5(f) represent the relative output power of the JR state at the interface with $n = (-5, -4)$ and at the interface with $n = (4, 5)$, respectively. As mentioned above, in the low-power regime (when $f < 0.2$) all the energy of the initial JR state at the interface with $n = (4, 5)$ is completely transferred to the JR state at the interface with $n = (-5, -4)$. As a result, the solid red curve is close to unity, whereas the dashed blue curve is close to zero. However, in the high-power regime (when $f > 1$) the situation radically changes, and all the energy just remains in the input JR state, and almost nothing is coupled to the other JR state. So like in fiber couplers, we can switch an optical beam from interface to interface at the output of the system, depending on its input power. So in general, the features of the linear coupling and nonlinear switching between two discrete JR states are quite similar to the ones between optical signals in symmetric fiber couplers (see Fig. 2.3 in [4]). The only significant difference between them is that in fiber couplers the coupling and switching happen just between two cores, whereas for JR states they happen between two interfaces.

The physical reason behind the nonlinear switching between two discrete JR states is similar to that for the one with symmetric fiber couplers [4]. The difference in the mode-propagation constants due to nonlinearity-based self-phase modulation (SPM) creates a relative phase shift between the two discrete JR states which results in incomplete power transfer between them. When the input power is high enough,

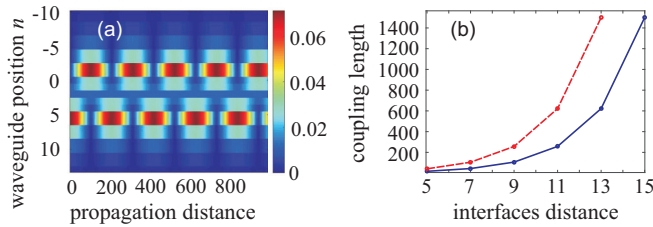


FIG. 6. (a) Coupling of two trivial states in the linear regime. (b) The linear coupling length L as a function of the center-to-center distance between two interfaces. The solid blue curve and the dashed red curve represent the cases with discrete JR states and with trivial states, respectively. Parameters are $|\sigma_1| = |\sigma_2| = |\sigma_3| = 1$, $\kappa = 1$, $\gamma = 0$.

the phase difference due to SPM is large enough, so the input discrete JR state is completely trapped during propagation in the same interface into which it was initially launched. Meanwhile, in the low-power linear regime the beams can be easily transferred between two interfaces. Therefore, as shown in Fig. 5(f), by adjusting the input power so that the factor f jumps from 0.25 to 0.48, at the output of the system with the length equal to the linear coupling length L one can switch almost all the input power to either the interface at $n = (-5, -4)$ or the interface at $n = (4, 5)$.

In Fig. 5 we demonstrate the coupling of two discrete JR states. These qualitative features are also true for two trivial states. As an example, in Fig. 6(a) we illustrate the coupling in the linear regime between two trivial states where the first and second interfaces are located at waveguides with $n = (-2, -1)$ and $n = (5, 6)$, respectively. So in this case the center-to-center distance between these two interfaces is $D = 7$. As seen in Fig. 6(a), the linear coupling length $L \simeq 105$ in this case. Surprisingly, this value L is almost the same as the one between two discrete JR states shown in Fig. 5(b) (where $L \simeq 106$), with the only exception being that the center-to-center distance between two interfaces in Figs. 5(b) and 6(a) is $D = 9$ and 7 , respectively.

Naturally, one can expect that the linear coupling length L varies exponentially as a function of the distance D between two interfaces. This is exactly the case, as illustrated in Fig. 6(b), where we plot the linear coupling length L as a function of the center-to-center distance D between two interfaces. The solid blue curve and the dashed red curve in

Fig. 6(b) represent the cases with the discrete JR states and trivial states, respectively. Because the two interfaces support localized states of the same type, the center-to-center distance D between them must be an odd number. It is also clearly shown in Fig. 6(b) that in the same conditions the coupling length between two discrete JR states is shorter than the one between two trivial states. So one can say that the coupling strength between two discrete JR states is stronger than that between two trivial states. As mentioned above, the coupling length L is almost the same if the interface distance $D = 9$ and 7 for discrete JR states and trivial states, respectively. This tendency is also true if $D = 7$ and 5 (the first and second values correspond to the discrete JR states and trivial states, respectively), $D = 9$ and 7 , $D = 11$ and 9 , $D = 13$ and 11 , $D = 15$ and 13 , and so on. The physical reasons behind this tendency are still not clear to us.

VI. CONCLUSIONS

In conclusion, we demonstrated numerically that two localized states of different types in interfaced binary waveguide arrays practically do not interact with each other, even though they are located quite close to each other. This feature can be used to protect one localized state from coupling to the other localized state of a different type and can present an efficient way to robustly guide optical signals in a network where various channels are tightly distributed. On the contrary, two localized states of the same type can strongly couple to each other in the linear regime and show a switching effect like in well-known symmetric fiber couplers by changing the input power. Our findings show that a system created by some BWAs where adjacent BWAs have opposite propagation mismatches can serve as a classical simulator to study the interaction between quantum relativistic JR states and between trivial states as well. This interaction can potentially be used for optical switching, coupling, and robust guiding in photonic integrated circuits.

ACKNOWLEDGMENTS

This research is funded by the Vietnam National Foundation for Science and Technology Development (NAFOSTED) under Grant No. 103.03-2019.03.

- [1] D. N. Christodoulides, F. Lederer, and Y. Silberberg, *Nature (London)* **424**, 817 (2003).
- [2] A. L. Jones, *J. Opt. Soc. Am.* **55**, 261 (1965).
- [3] D. N. Christodoulides and R. I. Joseph, *Opt. Lett.* **13**, 794 (1988).
- [4] G. P. Agrawal, *Applications of Nonlinear Fiber Optics*, 2nd ed. (Academic, New York, 2008).
- [5] Tr. X. Tran and F. Biancalana, *Phys. Rev. Lett.* **110**, 113903 (2013).
- [6] Tr. X. Tran and F. Biancalana, *Opt. Express* **21**, 17539 (2013).
- [7] T. X. Tran, D. C. Duong, and F. Biancalana, *Phys. Rev. A* **89**, 013826 (2014).
- [8] T. Pertsch, P. Dannberg, W. Elflein, A. Bräuer, and F. Lederer, *Phys. Rev. Lett.* **83**, 4752 (1999).
- [9] M. Ghulinyan, C. J. Oton, Z. Gaburro, L. Pavesi, C. Toninelli, and D. S. Wiersma, *Phys. Rev. Lett.* **94**, 127401 (2005).
- [10] S. Longhi, *Opt. Lett.* **35**, 235 (2010).
- [11] F. Dreisow, M. Heinrich, R. Keil, A. Tünnermann, S. Nolte, S. Longhi, and A. Szameit, *Phys. Rev. Lett.* **105**, 143902 (2010).
- [12] S. Longhi, *Phys. Rev. B* **81**, 075102 (2010).
- [13] F. Dreisow, R. Keil, A. Tünnermann, S. Nolte, S. Longhi, and A. Szameit, *Europhys. Lett.* **97**, 10008 (2012).
- [14] T. X. Tran, S. Longhi, and F. Biancalana, *Ann. Phys. (NY)* **340**, 179 (2014).

- [15] T. X. Tran, X. N. Nguyen, and D. C. Duong, *J. Opt. Soc. Am. B* **31**, 1132 (2014).
- [16] T. X. Tran and D. C. Duong, *Ann. Phys. (NY)* **361**, 501 (2015).
- [17] T. X. Tran, X. N. Nguyen, and F. Biancalana, *Phys. Rev. A* **91**, 023814 (2015).
- [18] T. X. Tran and D. C. Duong, *Chaos* **28**, 013112 (2018).
- [19] T. X. Tran, *J. Opt. Soc. Am. B* **36**, 2001 (2019).
- [20] A. A. Sukhorukov and Y. S. Kivshar, *Opt. Lett.* **27**, 2112 (2002).
- [21] A. A. Sukhorukov and Y. S. Kivshar, *Opt. Lett.* **28**, 2345 (2003).
- [22] M. Conforti, C. De Angelis, and T. R. Akylas, *Phys. Rev. A* **83**, 043822 (2011).
- [23] R. Morandotti, D. Mandelik, Y. Silberberg, J. S. Aitchison, M. Sorel, D. N. Christodoulides, A. A. Sukhorukov, and Y. S. Kivshar, *Opt. Lett.* **29**, 2890 (2004).
- [24] M. I. Molina, I. L. Garanovich, A. A. Sukhorukov, and Y. S. Kivshar, *Opt. Lett.* **31**, 2332 (2006).
- [25] R. Jackiw and C. Rebbi, *Phys. Rev. D* **13**, 3398 (1976).
- [26] T. X. Tran and F. Biancalana, *Phys. Rev. A* **96**, 013831 (2017).
- [27] N. N. Rosanov and T. X. Tran, *Chaos* **17**, 037114 (2007).
- [28] T. X. Tran, Hue M. Nguyen, and D. C. Duong, *Phys. Rev. A* **100**, 053849 (2019).
- [29] T. X. Tran, *Chaos* **30**, 063134 (2020).
- [30] T. X. Tran, D. C. Duong, and F. Biancalana, *J. Lightwave Technol.* **35**, 5092 (2017).
- [31] R. B. Laughlin, *Rev. Mod. Phys.* **71**, 863 (1999).
- [32] M. Z. Hasan and C. L. Kane, *Rev. Mod. Phys.* **82**, 3045 (2010).
- [33] M. C. Rechtsman, J. M. Zeuner, Y. Plotnik, Y. Lumer, D. Podolsky, F. Dreisow, S. Nolte, M. Segev, and A. Szameit, *Nature (London)* **496**, 196 (2013).
- [34] T. X. Tran, *J. Opt. Soc. Am. B* **36**, 2559 (2019).
- [35] N. Malkova, I. Hromada, X. Wang, G. Bryant, and Z. Chen, *Opt. Lett.* **34**, 1633 (2009).
- [36] A. Blanco-Redondo, I. Andonegui, M. J. Collins, G. Harari, Y. Lumer, M. C. Rechtsman, B. J. Eggleton, and M. Segev, *Phys. Rev. Lett.* **116**, 163901 (2016).
- [37] J. Ruostekoski, G. V. Dunne, and J. Javanainen, *Phys. Rev. Lett.* **88**, 180401 (2002).
- [38] T. Yefsah, A. T. Sommer, M. J. H. Ku, L. W. Cheuk, W. Ji, W. S. Bakr, and M. W. Zwierlein, *Nature (London)* **499**, 426 (2013).
- [39] D. G. Angelakis, P. Das, and C. Noh, *Sci. Rep.* **4**, 6110 (2014).
- [40] F. F. Li, H. X. Wang, Z. Xiong, Q. Lou, P. Chen, R. X. Wu, Y. Poo, J. H. Jiang, and S. John, *Nat. Commun.* **9**, 2462 (2018).
- [41] A. A. Gorlach, D. V. Zhirihin, A. P. Slobozhanyuk, A. B. Khanikaev, and M. A. Gorlach, *Phys. Rev. B* **99**, 205122 (2019).
- [42] C. Xu, P. Zhang, D. Zhao, H. Guo, M. Huang, and S. Ke, *Appl. Sci.* **9**, 4152 (2019).
- [43] R. Morandotti, U. Peschel, J. S. Aitchison, H. S. Eisenberg, and Y. Silberberg, *Phys. Rev. Lett.* **83**, 4756 (1999).